Heliyon 10 (2024) e34755

Contents lists available at ScienceDirect

Heliyon

journal homepage: www.cell.com/heliyon

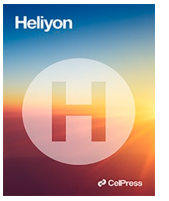

Research article

The involvement of epidural fat in ossification of the ligamentum flavum: From the perspective of exosomal proteome

Chao Wang [a,1,**], Yida Wang [a,1], Weihang Zhu [a], Qian Tang [b], Xuekang Wang [b], Lu Zhang [c,*]

[a] Department of Spine Surgery, The Affiliated Hospital of Qingdao University, Qingdao, China
[b] Department of Clinical Laboratory, The Affiliated Hospital of Qingdao University, Qingdao, China
[c] Medical Research Center, The Affiliated Hospital of Qingdao University, Qingdao, China

ARTICLE INFO

Keywords:
Ossification of the ligamentum flavum
Epidural fat
Exosome
Proteomics

ABSTRACT

Ossification of the ligamentum flavum (OLF) is the primary etiology of thoracic spinal stenosis. The functional properties of epidural fat (EF), an adipose tissue located in close proximity to ligamentum flavum (LF), have been scarcely investigated. The metabolic state of adipocytes significantly influences their functionality, and exosomes play a pivotal role in intercellular communication. This study aimed to investigate the role of EF-derived exosomes in OLF and characterize their protein profile by proteomics analysis. Our findings demonstrate that exosomes obtained from EF adjacent to OLF possess the ability to enhance osteogenesis of fibroblasts *in vitro*. Furthermore, proteomics analysis revealed metabolic dysfunction in EF adipocytes and identified lactate dehydrogenase A (LDHA) as a potential mediator involved in the development of OLF. This study provides new insights into the pathogenic mechanism underlying OLF and offers a theoretical basis for preventing and treating ligament ossification.

1. Introduction

The ligamentum flavum (LF), situated dorsally within the spinal canal, is a crucial connective tissue that plays an essential role in maintaining spinal stability. In addition to providing physical protection to the dural sac and spinal cord, it effectively restricts excessive flexion of the vertebrae under physiological conditions [1]. Ossification of the ligamentum flavum (OLF) typically occurs in the thoracic spine, resulting in spinal cord compression and subsequent manifestation of severe neurological dysfunction [2]. The etiology of OLF is postulated to involve a synergistic interplay among genetic factors, endocrine-metabolic abnormalities, mechanical stress, and other contributory elements; nevertheless, the precise pathogenic mechanisms remain elusive [3,4]. Our previous studies have revealed that advanced age and elevated body mass index (BMI) are established risk factors for thoracic ossification of the LF [5]. However, the underlying mechanism linking obesity or systemic metabolic dysfunction to the progression of OLF remains poorly elucidated.

It is widely acknowledged that adipose tissue undergoes substantial metabolic modifications, which subsequently exert a pivotal impact on insulin sensitivity, lipid synthesis, and the inflammatory response. The epidural fat (EF) is a type of adipose tissue that is

* Corresponding author.
** Corresponding author.
E-mail addresses: dr_wangchao@hotmail.com (C. Wang), zhanglu2022@qdu.edu.cn (L. Zhang).
[1] These authors contributed equally to this work.

https://doi.org/10.1016/j.heliyon.2024.e34755
Received 5 February 2024; Received in revised form 18 June 2024; Accepted 16 July 2024
Available online 22 July 2024

distributed within the epidural space and is anatomically adjacent to the LF. It cushions the vibrations of the dural sac to protect the contents of the spinal canal from the impact of the mobile spine [6]. For a long period, EF was disregarded and even deemed dispensable by spine surgeons during extensive decompression surgeries. However, recent research has led to a shift in perspective and an updated perception of the EF [7,8]. The functional investigation of EF-derived mesenchymal stem cells (EF-MSCs) also elucidates a pivotal role within the local microenvironment [9]. The close proximity of EF to the LF within the anatomical space has prompted our speculation regarding the potential involvement of EF in the occurrence and progression of OLF. Recently, Liu's group has made a novel discovery indicating that the EF adjacent to the ossified LF exhibits a fibrotic phenotype, enhanced vascularization and inflammation. This finding suggests an active involvement of EF in OLF through an inflammation-dependent paracrine mechanism [10]. However, the interaction pattern between EF and LF, as well as the underlying mechanisms involved, remain unclear. Additionally, exosomes have garnered significant attention in recent years as a novel endogenous carrier system facilitating cellular interactions. The mounting evidence indicates that adipocyte-derived exosomes possess the ability to modulate diverse physiological functions including energy metabolism, inflammation, tumorigenesis, and insulin sensitivity [11,12]. The objective of this study was to investigate the involvement of EF in the progression of OLF through an exosome-dependent mechanism and analyze the proteomic characteristics of EF-derived exosomes, aiming to enhance our understanding of OLF pathogenesis and identify novel therapeutic targets for this disease.

2. Results

2.1. Morphological identification of EF in OLF and non-OLF patients

The flow chart illustrating the global experimental procedures is presented Fig. 1. Based on the canal occupation rate of the OLF on CT axial plane, OLF is classified into moderate OLF (M-OLF) and severe OLF (S-OLF) (Fig. 2A–B). Macroscopically, the EF is closely attached to the surface of the ossified LF (Fig. 2C). Further morphological analysis of the EF among different groups reveals a significant reduction in adipocyte size within the EF tissue adjacent to the ossified LF, as compared to normal tissue. However, no difference is observed between M-OLF and S-OLF groups (Fig. 2D).

2.2. Characterization of the exosomes from EF

Exosomes from EF with severe OLF (OLF-EFexo) and normal control EF (CON-EFexo) are extracted for further identification. By using transmission electron microscopy (TEM), distinct vesicle structures meeting the size criteria for exosomes were observed in visual fields of both groups (Fig. 3A). The vesicles' size was evaluated using nanoparticle tracking analyzer (NTA), revealing that the diameter of vesicles in OLF-EF was slightly smaller compared to the control group (118.1 ± 8.3 vs 128.7 ± 5.5 nm); however, this difference did not reach statistical significance (Fig. 3B). The Western blot analysis reveals the presence of tumor susceptibility gene 101 (TSG101) and CD9, which are established exosomal marker proteins, in the isolated extracellular vesicles (Fig. 3C). The above

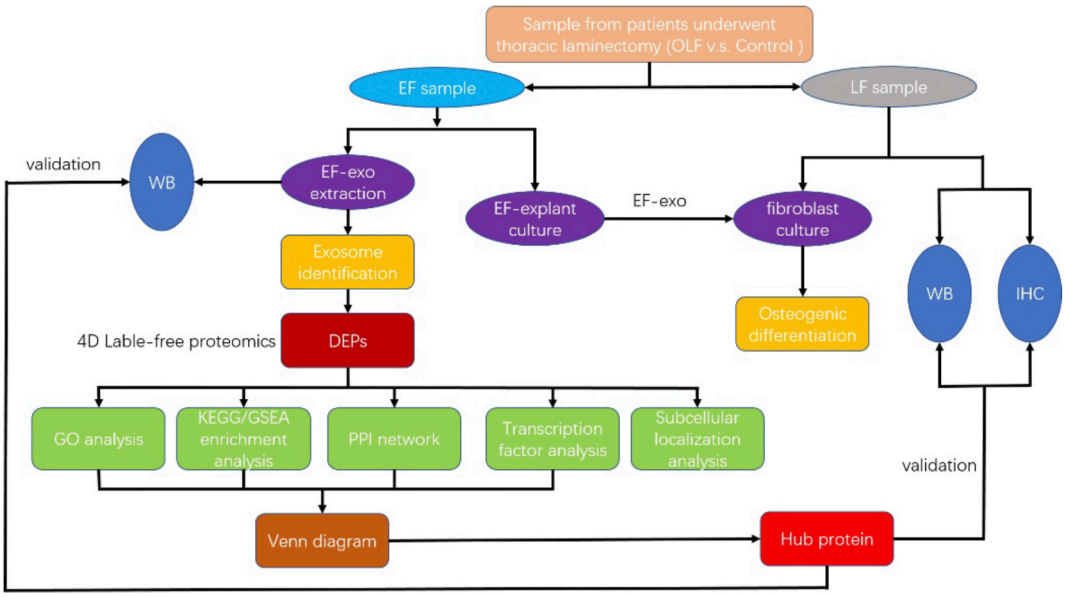

Fig. 1. Flowchart of the entire analysis. DEP, differentially expressed protein; EF, epidural fat; LF, ligamentum flavum; EF-exo, epidural fat-derived exosome; OLF, ossification of the ligamentum flavum; WB, Western blot; IHC, immunohistochemistry; GO, gene ontology; KEGG, Kyoto Encyclopedia of Genes and Genomes; GSEA, Gene Set Enrichment Analysis; PPI, protein-protein interaction.

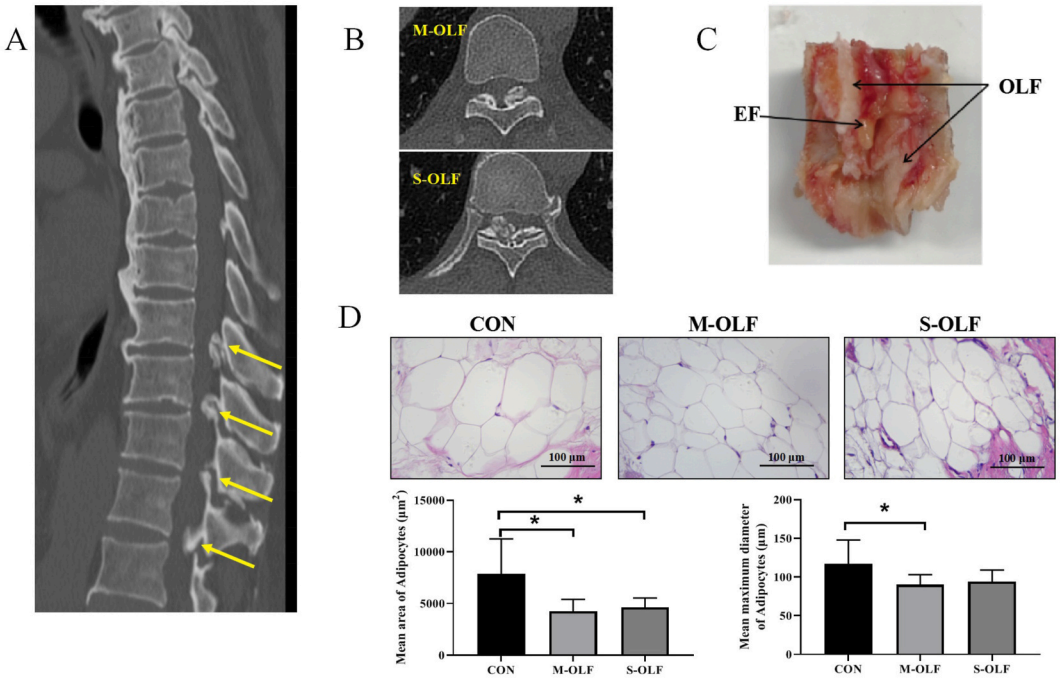

Fig. 2. EF morphology from the OLF patients. (A) Sagittal CT of typical OLF patients showed multiple ossified LF (arrow). (B) Typical manifestations of moderate and severe OLF on axial CT plane. (C) Anatomical relationship of LF and EF in a surgical resection specimen. (D) Representative HE staining images of EF and statistical results of adipocyte size. *$P < 0.05$.

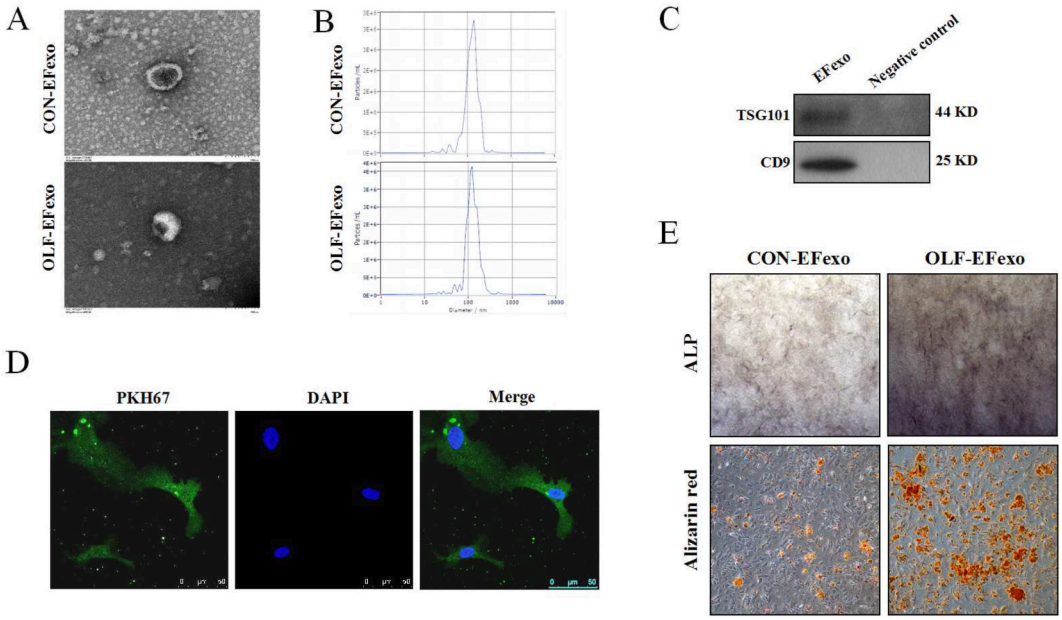

Fig. 3. Identification of EF-derived exosome and its osteogenic potential. (A) The typical vesicle structure of the exosomes seen under TEM. (B) Schematic diagram of the diameter distribution of exosomes in two groups displayed by nanoparticle tracking technology (NTA). (C) The expression of exosomal proteins TSG101 and CD9 shown by Western blot. (D) Distribution of PKH67 labeled exosomes in fibroblasts cultured *in vitro*. (E) With osteogenic induction, the fibroblasts cultured *in vitro* were incubated with EF-derived exosomes from the control and OLF groups, respectively. The ALP staining and Alizarin Red staining were subsequently performed.

findings demonstrate the successful isolation of exosomes from OLF-EF and CON-EF, with no significant disparity observed in terms of particle size between the two groups. Subsequently, EF-derived exosomes were labeled with the green fluorescent dye PKH67 and co-incubated with primary fibroblasts derived from LF. After a 2-h incubation period, it was evident that the fibroblasts exhibited uniform green fluorescence staining, indicating successful uptake of EF-derived exosomes (Fig. 3D). Interestingly, fibroblasts incubated with OLF-EFexo demonstrate an augmented osteogenic capacity compared to cells incubated with CON-EFexo, as evidenced by stronger ALP staining following a 14-day osteogenic induction. Moreover, the Alizarin Red staining results reveal that calcification in the OLF-EFexo group is more pronounced than that in the CON-EFexo group after 21 days.

2.3. Identification of differentially expressed proteins in OLF-EFexo and GO analysis

To further investigate the potential regulatory. mechanism of OLF-EFexo on the fibroblast osteogenic differentiation, we performed a 4D label-free quantitative proteomic analysis. A total of 1909 proteins were identified in the CON-EFexo group, while 1758 proteins were identified in the OLF-EFexo group; among them, 1703 proteins were commonly identified in both groups (Sup Fig). Notably, we found a total of 84 significantly differentially expressed proteins (DEPs) between OLF-EFexo and CON-EFexo (log_2[fold change] >1.5-fold and $P < 0.05$), including 18 up-regulated proteins and 66 down-regulated proteins (Fig. 4A–B, Supplementary Table). Gene ontology (GO) annotation and enrichment analysis are performed on these DEPs (Fig. 4C). For biological processes, DEPs are mainly enriched in isoleucine catabolic process, regulation of ATP biosynthesis, amino acid metabolism, and fatty acid oxidation (Fig. 4D). For cellular component (CC), DEPs are mainly enriched in mitochondria, including mitochondrial matrix, and mitochondrial inner membrane (Fig. 4E). For molecular function, DEPs are primarily enriched in adenylate kinase activity, as well as glucose transporter activity and protein kinase C (PKC) inhibitor activity.

2.4. KEGG pathway enrichment and GSEA analysis

According to KEGG (Kyoto Encyclopedia of Genes and Genomes) pathway annotation, the DEPs predominantly aggregates in metabolic pathways, secondary metabolite synthesis, and thermogenesis. Enrichment analysis reveals that the DEPs are significantly enriched in propanoate metabolism, thermogenesis, fatty acid metabolism, amino acid degradation and other relevant pathways (Fig. 5A–B). While the KEGG analysis lacks detailed information regarding the positive or negative regulation of specific pathways, the GSEA (Gene Set Enrichment Analysis) further reveals that the positively correlated DEPs are enriched mainly in ribosomes, proteasomes, and antigen presentation (Fig. 5C), while the negatively correlated DEPs were enriched in fatty acid metabolism pathway, tricarboxylic acid cycle (TCA) pathway, oxidative phosphorylation pathway, *etc*. (Fig. 5D).

2.5. Prediction of subcellular localization, transcription factor, and protein-protein interaction

The subcellular localization analysis of the DEPs reveals their predominant localization (over 45 %) at the mitochondria, followed by the cytosol and plasma membrane(Fig. 6A). The DEPs are subsequently annotated with the AnimalTFDB (Animal Transcription Factor Database) to determine their enriched transcription factor families. The top enriched transcription factor families identified are zing finger and BTB (ZBTB), signal transducer of activation (STAT) -bind, mad homology 1(MH1), and cold shock domain (CSD), respectively (Fig. 6B). Furthermore, ChEA3 (ChIP-X Enrichment Analysis 3) database was used to predict transcription factors

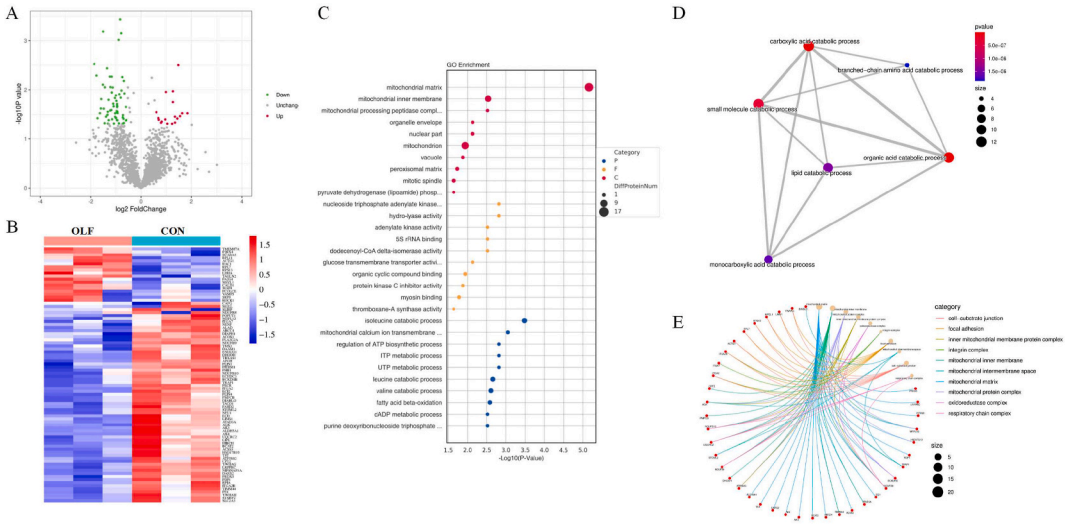

Fig. 4. Exosome proteomic results and GO analysis. (A)Volcano plots. (B) Heat map for the DEPs. (C) GO enrichment analysis of DEPs. (D) GO enrichment analysis for biological processes. (E) Chordal plots showed the category of cellular components in which the DEPs enriched.

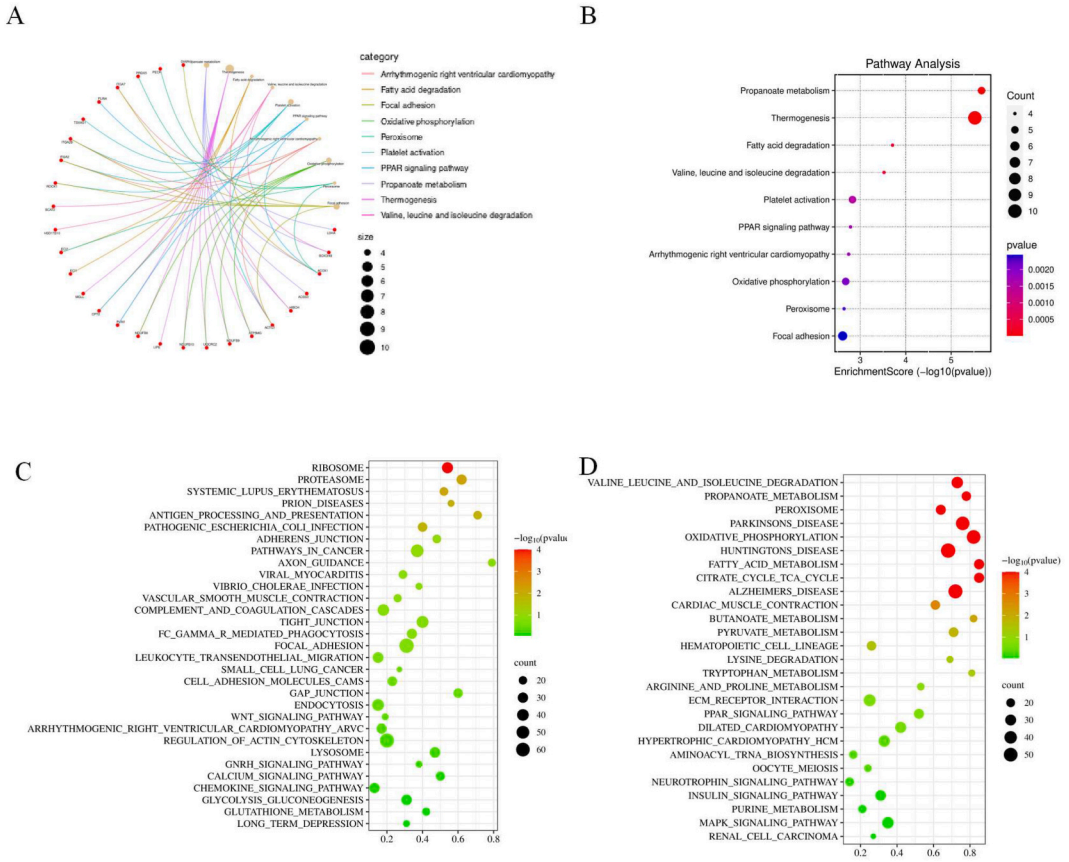

Fig. 5. KEGG and gene set enrichment analysis (GSEA). (A) Pathway chordal diagram of DEPs indicated by KEGG pathway annotation. (B) KEGG pathway enrichment analysis shown as bubble plot (top 10). (C) Results of GSEA analysis for positively correlated pathways (gene sets) in OLF-EFexo compared with CON-EFexo. (D) Results of GSEA analysis for negatively correlated pathways (gene sets) in OLF-EFexo compared with CON-EFexo.

implicated in the regulation of the DEPs, with prolactin regulatory element-binding (PREB), zinc finger-511 (ZNF511), and thanatos associated protein-4 (THAP4) emerging as the top three candidates (Fig. 6C). The subsequent analysis of protein-protein interactions (PPI) revealed that among the top 10 potential hub proteins, nine exhibited downregulation in OLF-EFexo, while only one protein, lactate dehydrogenase A (LDHA), demonstrated upregulation (Fig. 6D). We further used the Venn diagram to find the potential key proteins that are most likely to regulate this process by intersecting hub proteins in PPI network, the DEPs in the top one enriched term of the GO analysis (mitochondrial matrix), the targeted proteins of PREB (the top one upstream transcription factor predicted by ChEA), and the DEPs included in the top enriched pathway in KEGG (propanoate metabolism). As the result, interestingly, LDHA emerged as the sole protein within this intersection (Fig. 6E).

2.6. Validation of hub protein expression

To verify the above bioinformatics results and provide supports for the subsequent experiments, we further measured the exosomal expression of two predicted hub proteins, LDHA and prohibitin-1 (PHB1) by Western blot analysis (Fig. 7A). The results demonstrate a significant increase in LDHA expression in OLF-EFexo, while PHB1 expression is significantly decreased, consistent with the proteomic findings. We further analyzed the expression of LDHA in ossified and normal LF tissues to investigate the potential involvement of LDHA in OLF. The photomicrographs of sections stained by hematoxylin-eosin (HE), masson's trichrome staining (MT) and elastica van Gieson staining (EVG) all reveal an increasingly irregular structure and decomposition in OLF (Fig. 7B). In addition, we found that the level of LDHA was significantly increased in the OLF group by Western blot and immunohistochemistry (IHC) analysis (Fig. 7C–D).

3. Discussion

Traditionally, the EF is acknowledged as a physical cushion for the dural sac and neural structures, safeguarding them against external forces, while simultaneously facilitating the relative motion of the dural sac along the bony spine during flexion and extension [13]. Furthermore, EF has been regarded as a quiescent tissue with low metabolic activity and minimal response to both endogenous

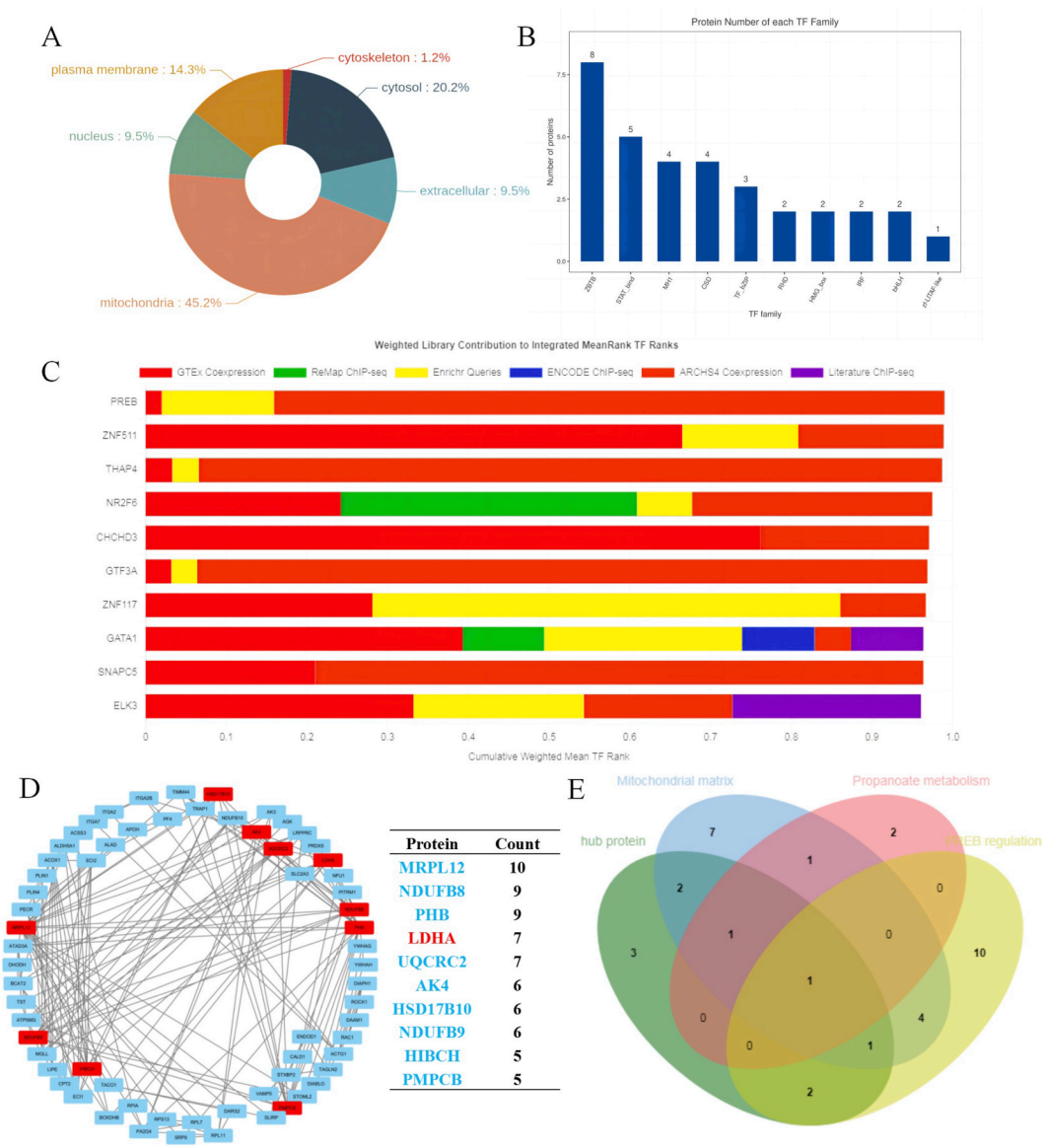

Fig. 6. Prediction of subcellular localization analysis, transcription factor analysis, and PPI. (A) Protein subcellular localization map; (B) Top 10 of transcription factors predicted by the AnimalTFDB3.0 database. (C) Top 10 of transcription factors predicted by the ChEA3 database. (D) PPI network diagram and the top 10 list (blue indicates downregulated proteins and red indicates upregulated proteins). (E) Venn diagram results.

and exogenous stimuli. Thereafter, the importance of EF was disregarded and even considered unnecessary by spine surgeons during extensive decompression surgeries. However, based on recent research findings, the perspective has undergone a transformation and the understanding of EF has been updated [8]. The functional investigation of EF and its derivatives has unveiled their pivotal roles in the local microenvironment and relevant disease models, encompassing spinal cord injury [14,15], dura injury/regeneration [16], disc degeneration [17], as well as ligament ossification [10].

Anatomically, the LF tissues, which attach to the posterior parts of the osseous spinal canal, is a close adjacent structure for the EF. Given the structural proximity, it is plausible that EF and LF tissues may exert direct functional influence on each other. A recent study conducted a comparison of the EF tissues adjacent to ossified or normal LF tissues [10]. The study suggests significant increase in fibrosis, vascularization, as well as infiltration of macrophages and B lymphocytes, in the histology of EF within the OLF group. This finding suggests potential dysfunction of adipocytes in EF tissue close to the ossified LF [18]. Additionally, the OLF group exhibits an augmented secretion of inflammatory factors and cytokines such as IL-6, TNF-α, and leptin by EF. Consistently, the level of phosphorylated STAT3 in the imminent ossified LF tissue is obviously up-regulated, indicating potential involvement of EF in the pathological process of OLF through an undisclosed paracrine signaling pathway. This finding enhances our understanding of OLF and encourages further investigation. Nevertheless, the precise influence of EF on ligament ossification remains predominantly

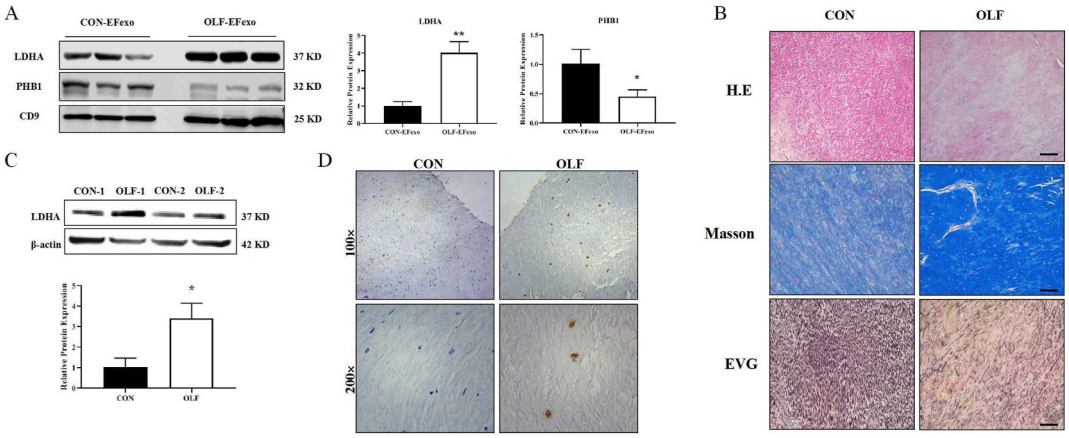

Fig. 7. Validation results of protein expression. (A) Western blot images and statistical results of LDHA and PHB1 from EF-derived exosomes in the control and OLF groups. *$P < 0.05$. (B) Representative morphology images of LF sections. Bar = 100 μm. (C) Western blot results and statistical plot of LDHA expression in the non-ossified and ossified LF tissues. *$P < 0.05$. (D) Representative IHC images of LDHA expression in the non-ossified and ossified LF tissues.

unexplored.

In recent years, exosomes have garnered significant attention as a novel endogenous carrier system facilitating cellular interactions. Mounting evidence has demonstrated the regulatory role of adipose tissue-derived exosomes in energy metabolism, inflammation, tumorigenesis, and insulin sensitivity [11,12]. In this study, we found that although with no obvious difference in size compared to normal controls, exosomes derived from EF adjacent to OLF tissues could promote osteogenesis in cultured LF-derived fibroblasts *in vitro*. This discovery represents the first elucidation on the role of EF tissue in OLF from an exosomal perspective, highlighting the potential translational applications for targeting EF in the prevention and treatment of OLF.

Exosomes can safeguard the transported cargo against degradation and facilitate intercellular material transfer through autocrine, paracrine, and endocrine mechanisms. It is noteworthy that the contents encapsulated within exosomes exhibit remarkable heterogeneity, contingent upon the donor cell origin and underlying pathophysiological conditions. In this study, we present a comprehensive analysis of proteomic changes in EF-derived exosomes during OLF for the first time. Based on the previous research, EF in OLF manifests more obvious tissue fibrosis and vascularization compared to the control [10], which is similar to the manifestations of adipocytes with mitochondrial dysfunction, endocrine dysregulation, and extracellular remodeling in pathological obesity [19]. In conjunction with the findings from the integrated bioinformatic algorithms in this study, it is postulated that mitochondrial dysfunction within EF may potentially contribute to the pathogenesis of OLF. In addition, the systemic effects of adipocyte dysfunction may also contribute to this pathogenesis under pathological conditions such as obesity and metabolic abnormalities. Further meticulously designed *in vivo* and *in vitro* experiments are warranted to substantiate the hypothesis.

Transcription factors possess the capacity to initiate and regulate transcription of a wide range of genes essential for maintaining normal physiological functions. Consequently, disruption of these interactions may contribute to the development of tissue-specific pathological phenotypes [20]. In this study, we performed two bioinformatic methods for the prediction of transcription factors. The AnimalTFDB3.0 database was utilized for assessing the transcription factor families among the DEPs, while the ChEA3 database was employed to predict the upstream transcription factors of these DEPs. The results of AnimalTFDB revealed many transcription factors previously reported to be associated with heterotopic ossification. For example, JAK-STAT signaling pathway plays an important role in inflammation-mediated osteogenic transformation. The JAK/STAT signaling pathway exhibits a positive correlation with the thickness of the LF [21]. The IL-6 cytokine serves as the principal activator of the STAT pathway, which has been previously demonstrated to be implicated in thoracic OLF [22]. STAT3 signaling pathway also serves as the central mediator underlying the osteogenic effect of leptin in OLF cells [23]. In addition, the MH1 domain plays a crucial role in the functional regulation of the Smad family, which is extensively implicated in BMP2-mediated osteogenesis [24,25]. Moreover, Rel homology domain (RHD) highlights the potential involvement of NF-kB in this process. Thus, we postulated that the presence of proteins encapsulated within EFexo may exert influence on the process of OLF via these particular pathways. PREB was ranked the first transcription factor in the prediction analysis of upstream transcription factors that might regulate these DEPs. The hormone prolactin plays a crucial role in regulating glucose and lipid metabolism, maintaining endothelial function, contributing to obesity development, and potentially influencing cardiovascular mortality [26]. PREB protein has been identified as a factor that regulates insulin gene expression in the pancreas. Besides, PREB potentially contributes to the regulation of adiponectin gene transcription in adipocytes, in response to cAMP activation [27]. The involvement of PREB implies that EF may serve as a highly sensitive indicator of systemic metabolic status and exert influence on the occurrence and progression of OLF.

Glucose glycolysis is the primary metabolic pathway utilized by osteoblasts and their progenitors for energy production. Even in the presence of adequate oxygen, a significant portion of glucose undergoes lactate metabolism during osteogenic differentiation, which is commonly referred to as aerobic glycolysis [28]. During OLF formation, the lack of blood vessels and hypoxic stimulation in the tissue

environment, coupled with the high demand for constant production of collagen, glycosaminoglycans and other substrates, lead to massive ATP consumption. In addition, it has been found in OLF clinical specimens that degenerative ligaments are often accompanied by the hypertrophy of the whole LF. In comparison to fibroblasts derived from normal LF, OLF-derived fibroblasts exhibit enhanced *in vitro* proliferation [29]. The above evidence indicates that OLF formation requires a huge energy supply. Similar to osteoblasts and others, LF-derived fibroblasts have a highly glycolytic metabolic pattern [30]. Through metabolomics and transcriptome analysis, Li J et al. found that glycolysis/glycogen production pathway was significantly activated in OLF [31]. The enzyme LDHA plays a pivotal role as an oxidoreductase in the glycolytic pathway across various organisms, facilitating the conversion of pyruvate to lactate during the final step of anaerobic glycolysis. During the process of osteogenic differentiation, there was a gradual increase in LDHA expression, intracellular lactate levels, and histone lactylation levels. Knockdown of LDHA resulted in reduced formation of mineralized nodules and decreased ALP activity in osteoblasts [32]. However, the involvement of LDHA in OLF has not been previously documented. In this study, we firstly verified the expression of LDHA in LF tissues and found that the expression of LDHA in OLF was significantly higher than that in the control group. Accordingly, we hypothesize that LDHA-catalyzed reaction may serve as a pivotal regulator in the osteogenesis of LF fibroblasts. EFexo could potentially facilitate the intracellular delivery of LDHA to fibroblasts, thereby inducing energy metabolism disorders and consequently promoting the ossification process of the LF. Further experiments are required to substantiate the role of EF-derived exosomes in mediating glucose metabolism in LF cells, elucidate the precise mechanism underlying their regulation of LF homeostasis, and offer novel targets and strategies for disease treatment.

In conclusion, we observe that EF-derived exosomes possess the ability to enhance osteogenic differentiation of LF fibroblasts, suggesting a potential role for EF-derived exosomes in mediating functional communication between EF and LF. Based on the proteomics results and bioinformatics analysis, we hypothesize that LDHA may serve as a pivotal mediator in EF-mediated regulation of LF osteogenic differentiation, while dysfunction of EF could potentially act as an initiating factor for OLF development induced by metabolic disorders. The finding of this study not only facilitates the comprehension of OLF mechanisms but also holds promise for identifying novel therapeutic targets for OLF and other ectopic ossification disorders.

4. Materials and methods

4.1. Tissue collection

LF and adjacent EF tissues were both obtained from OLF and control patients who underwent laminectomy and decompression surgery in the department of spinal surgery, the affiliated hospital of Qingdao university. Informed consents were routinely collected from all patients. OLF is diagnosed based on the combination of the clinical manifestations and imaging characteristics. According to the invasion rate of ossification in the spinal canal, OLF is divided into moderate OLF (occupancy rate $<$50 %) and severe OLF (occupation rate $\geq$50 %). The control samples were collected from patients with thoracic vertebral fracture, thoracic intervertebral disc herniation, or benign subdural tumor, with no imaging signs of OLF. The obtained LF and EF tissues were carefully separated for further experiments.

4.2. Section staining and IHC

The morphology of EF was assessed using HE staining. Adipocyte size was determined by calculating the average maximal diameter and mean area of adipocytes in all measured fields. MT and EVG were performed according to the manufacturer's protocol. To investigate the LDHA expression level, paraffin sections of LF were incubated with a rabbit primary anti-LDHA antibody (#3582, CST, USA), followed by horseradish peroxidase-conjugated goat anti-rabbit IgG and 3,3-diaminobenzidine. All images were analyzed using ImageJ software.

4.3. Extraction and identification of exosomes from EF

The culture medium containing exosomes obtained from EF was transferred to 15 mL centrifuge tubes. Then it was centrifuged at 2000 g/min for 30 min at 4 °C, and the supernatant was collected. The supernatant was subsequently centrifuged at 10,000 g/min for 45 min at 4 °C to remove larger vesicles. The supernatant was collected and transferred to an ultra-centrifuge tube (30 mL tube), centrifuged at 110,000 g/min for 75 min and the supernatant was discarded. The precipitate was resuspended in precooled 1 mL 1 × PBS, diluted to 15 mL in 1 × PBS, filtered with 0.22 μm filter membrane, and transferred to an ultra-centrifuge tube. Then, it was centrifuged at 100,000 g/min for 75 min at 4 °C, and the supernatant was discarded. The exosome precipitate was resuspended in 200 μL 1 × PBS, frozen stored at −80 °C.

Exosome identification was carried out using various methods. Exosome morphology was detected using TEM (FEI, Tecnai G2 Spirit BioTwin). Exosome diameter was measured by using a nanoparticle tracking analyzer (PARTICLE METRIX, ZetaVIEW S/N 17–310) according to the manufacturer's protocol. Western blot was used to measure the expression of TSG101 and CD9 in the extracted samples.

4.4. EF explants culture

The surgically removed EF samples were thoroughly washed in a cold, sterile PBS solution to eliminate any visible connective tissue and blood clots. The EF samples were subsequently cut into small pieces and placed in DMEM for 1 h at 37 °C and 5 % CO_2. After 1 h,

the EF samples were seeded to a 24-well culture plate (wet weight 10 mg/well). Explants were cultured in DMEM containing 100 U/mL penicillin G and 100 mg/mL streptomycin for 24 h, and the conditional medium was collected for exosome extraction, identification, and preservation until use.

4.5. LF-derived primary fibroblasts culture

The collected LF tissue was cut into pieces approximately 1 mm^3 in size, placed in a 25 mm^2 culture flask and then transferred into an incubator. After 2–3 h, DMEM medium containing 10 % FBS was slowly added into the flask. The cells were digested by 0.25 % trypsin and then passaged after approximately 80 % cellular confluence. The P2 and P3 cells were stored for further experiments. During osteogenic induction, the fibroblasts were cultured with an osteogenic medium (50 μM ascorbic acid, 10 nM β-glycerophosphate, and 10 nM dexamethasone). When conducting exosome experiments, an exosome concentration of 10 μg/mL was selected for the experiments. Osteogenic inducing stimuli and exosomes were re-added every two days as the medium was changed.

4.6. Protein extraction and western blot analysis

Exosomes or cells were thawed at 37 °C and rapidly added into 5 × RIPA lysate, mixed, and lysed on ice for 30 min. Protein concentration was determined by the BCA method. The absorbance values were detected at OD562 nm on a microplate reader and was then recorded. The protein extracts were resolved using 12 % SDS-PAGE, followed by incubation of the membranes with primary antibody and HRP-conjugated secondary antibodies. The chemiluminiscence signal was detected using the Odyssey infrared imaging system (LI-COR Biosciences, Lincoln, Neb).

4.7. Detection of exosome ingestion

Exosomes were marked by PKH67 fluorescent labeling kit (MINI67, Millipore). 10 μL exosomes were incubated with 4 mL PKH67 dye in diluent C for 4 min and an equal amount of FBS was added to terminate the experiment. PKH67-labeled exosomes were extracted using the isolation reagent and then incubated with LF-derived fibroblasts for 2 h, after which exosome intake was visualized using a confocal microscopy (Nicon, Japan).

4.8. ALP staining

After osteogenic induction of the fibroblasts for 14 days, the culture medium was discarded and the fibroblasts were washed three times with PBS, 4 % paraformaldehyde for fixation. Then the cells were washed 3 times again and subsequently incubated with ALP dye (modified Gomori Ca–CoS method) solution (Solarbio, China) in dark at 37 °C for 15 min. The positive result exhibited dark brown precipitates.

4.9. Alizarin Red staining

After osteogenic induction of the fibroblasts for three weeks, the culture medium was discarded and the fibroblasts were washed three times with PBS, fixed with 4 % paraformaldehyde for 10 min, and washed three times again with PBS. One milliliter of Alizarin Red solution (1 %) was added and incubated for 30 min. After discarding the solution, wash the cells with double distilled water to remove the floating color. Calcified nodules can be stained red under the light microscope.

4.10. Exosome proteomics sample preparation

The frozen EF tissue was grinded in liquid nitrogen and 1 mL SDT lysate (4 % SDS, 100 mM Tris-HCl, pH 7.6) was added to each sample. After boiled in water for 10 min, the lysate was centrifuged at 14,000 g/min for 15 min to obtain the protein supernatants. Protein concentration was measured by BCA assay, and 50 μg protein was taken for further proteomic study. DTT was added to form a solution with a final protein concentration of 100 mM, which was boiled for 5 min. Then the detergent, DTT and other low-molecular-weight components were removed using UA buffer (8 M Urea, 150 mM Tris-HCl, pH 8.5) by repeated ultrafiltration (Sartorius, 30 kD). Then 100 μL iodoacetamide (100 mM IAA in buffer) was added for alkylation and the samples were incubated for 30 min in darkness. The filters were washed with 100 μL buffer three times and then 100 μL 50 mM NH_4HCO_3 buffer twice. Finally, the protein suspensions were digested with 4 μg trypsin (Promega) in 40 μL 50 mM NH_4HCO_3 buffer overnight at 37 °C, and the resulting peptides were collected as a filtrate. The peptide segment was desalted by C18 column. The dried peptides were dissolved in 0.1 % formic acid and estimated by UV light spectral density at 280 nm using an extinctions coefficient of 1.1 that was calculated on the basis of the frequency of tryptophan and tyrosine in vertebrate proteins.

4.11. Mass spectrometry analysis

Samples were analyzed on a nanoElute (Bruker, Bremen, Germany) coupled to a timsTOF Pro (Bruker, Bremen, Germany) equipped with a CaptiveSpray source. Peptides were separated on a 25 cm × 75 μm analytical column, 1.6 μm C18 beads with a packed emitter tip (IonOpticks, Australia). The column temperature was maintained at 50 °C using an integrated column oven (Sonation GmbH,

Germany). The column was equilibrated using 4 column volumes before loading sample in 100 % buffer A (99.9 % MilliQ water, 0.1 % FA). Samples were separated at 300 nl/min using a linear gradient as follows: 1.5 h' gradient, 2–22 % buffer B for 75 min, 22–37 % buffer B for 5 min, 37–80 % buffer B for 5 min, hold in 80 % buffer B for 5 min. The timsTOF Pro (Bruker, Bremen, Germany) was operated in PASEF mode. Mass Range 100–1700 m/z, 1/K0 Start 0.75 V s/cm2 End 1.4 V s/cm2, Ramp time 100 ms, Lock Duty Cycle to 100 %, Capillary Voltage 1500 V, Dry Gas 3 L/min, Dry Temp 180 °C, PASEF settings: 10 MS/MS scans (total cycle time 1.16 s), charge range 0–5, active exclusion for 0.5 min, Scheduling Target intensity 10000, Intensity threshold 2500, CID collision energy 20–59 eV.2.10.3 Data analysis.

The MS data were analyzed using MaxQuant software version 1.6.17.0. MS data were searched against the UniProt database. An initial search was set at a precursor mass window of 10 ppm. The search followed an enzymatic cleavage rule of Trypsin/P and allowed maximal two missed cleavage sites and a mass tolerance of 40 ppm for fragment ions. Carbamidomethylation of cysteines was defined as fixed modification, while protein N-terminal acetylation and methionine oxidation were defined as variable modifications for database searching. The cutoff of global false discovery rate (FDR) for peptide and protein identification was set to 0.01. Protein abundance was calculated on the basis of the normalized spectral protein intensity (LFQ intensity). Proteins which fold change >1.5 and $P < 0.05$ were considered to be differentially expressed proteins.

5. Gene ontology (GO) annotation

At first, all protein sequences were aligned to the UniProt database using NCBI BLAST+ (ncbi-blast-2.3.0+) on the Linux server, only the sequences in top 10 and E-value≤1e-3 were kept. Secondly, select the GO term (database version: go_20190701.obo) of the sequence with top Bit-Score by Blast2GO. Then, completed the annotation from GO terms to proteins by Blast2GO Command Line. After the elementary annotation, InterProScan were used to search EBI database by motif and then add the functional information of motif to proteins to improve annotation. Then further improvement of annotation and connection between GO terms were carried out by ANNEX. Fisher's exact test were used to enrich GO terms by comparing the number of differentially expressed proteins and total proteins correlated to GO terms.

5.1. KEGG pathway and GSEA

Pathway analysis was performed using KEGG database (database version: KO_INFO_END.txt (2022.01.25)). Fisher's exact test were used to identify the significantly enriched pathways by comparing the number of differentially expressed proteins and total proteins correlated to pathways. Subsequently, a GSEA was performed according to the well-established manufactures introduced by previous researches (http://software.broadinstitute.org/gsea/index.jsp) [33,34].

5.2. Protein-protein interaction (PPI) network analysis

The target protein ID was used to find the direct or indirect interaction relationship network with the target protein in the STRING database (download link: string-db.org), and the AnyChart software (V8.11.0.1934) was used Generate the interaction network analysis results. The data acquired in STRING were then imported into Cytoscape (version 3.7.1), which is an open source software for visualizing PPI and combining PPI data with attributing data. Based on the frequency of occurrence in the twelve algorithms from Cytoscape, hub genes considering for the specific cell type were screened. Western blot was performed to preliminary validate the analysis results of concerned proteins.

5.3. Analysis of the subcellular localization

The commonly used prediction software WoLF PSORT (download link:wolfpsort.hgc.jp) was used to perform subcellular localization prediction on differential proteins. The software is based on sorting signals, amino acid composition, and functional motifs, to convert the protein sequences into digital localization features. The KNN (k-Nearest Neighbor) classifier was subsequently used to predict the subcellular localization of protein.

5.4. Transcription factor analysis

The AnimalTFDB database was used to perform transcription factor prediction analysis on identified total and differential proteins. Moreover, we applied ChEA3 transcription factor enrichment analysis tool to predict and rank upstream transcription factors related to differential protein gene sets.

5.5. Statistical analysis

All results are expressed as mean ± standard error of the mean (SEM). Statistical analyses involved use of GraphPad Prism 5.0 (GraphPad Software Inc, La Jolla, CA). A $P < 0.05$ was considered statistically significant.

Ethics statement

This study was approved by the ethical committee of the affiliated hospital of Qingdao university (Approval No. QYFY-WZLL-28461). Informed consent was obtained from all patients for the publication of all images, clinical data and other data included in the manuscript. The study complies with all regulations.

Data availability statement

Data will be made available on request.

Funding

This work was supported by the National Natural Science Foundation of China (81902209).

CRediT authorship contribution statement

Chao Wang: Funding acquisition, Conceptualization. **Yida Wang:** Writing – original draft, Investigation. **Weihang Zhu:** Methodology. **Qian Tang:** Methodology. **Xuekang Wang:** Methodology, Investigation. **Lu Zhang:** Writing – review & editing, Conceptualization.

Declaration of competing interest

The authors declare the following financial interests/personal relationships which may be considered as potential competing interests:Chao Wang reports financial support was provided by the National Natural Science of China. If there are other authors, they declare that they have no known competing financial interests or personal relationships that could have appeared to influence the work reported in this paper.

Appendix A. Supplementary data

Supplementary data to this article can be found online at https://doi.org/10.1016/j.heliyon.2024.e34755.

References

[1] V.A. Byvaltsev, A.A. Kalinin, P.A. Hernandez, V.V. Shepelev, Y.Y. Pestryakov, M.A. Aliyev, M.B. Giers, Molecular and genetic mechanisms of spinal stenosis formation: systematic review, Int. J. Mol. Sci. 23 (2022) 13479.
[2] G. Chen, T. Fan, X. Yang, C. Sun, D. Fan, Z. Chen, The prevalence and clinical characteristics of thoracic spinal stenosis: a systematic review, Eur. Spine J. : official publication of the European Spine Society, the European Spinal Deformity Society, and the European Section of the Cervical Spine Research Society 29 (2020) 2164–2172.
[3] D.K. Ahn, S. Lee, S.H. Moon, K.H. Boo, B.K. Chang, J.I. Lee, Ossification of the ligamentum flavum, Asian Spine J. 8 (2014) 89–96.
[4] A. Nouri, L. Tetreault, A. Singh, S.K. Karadimas, M.G. Fehlings, Degenerative cervical myelopathy: epidemiology, genetics, and pathogenesis, Spine 40 (2015) E675–E693.
[5] H. Zhang, N. Deng, L. Zhang, L. Zhang, C. Wang, Clinical risk factors for thoracic ossification of the ligamentum flavum: a cross-sectional study based on spinal thoracic three-dimensional computerized tomography, Risk Manag. Healthc. Pol. 15 (2022) 1065–1072.
[6] M.A. Reina, C.D. Franco, A. López, D.A. Ja, A. van Zundert, Clinical implications of epidural fat in the spinal canal. A scanning electron microscopic study, Acta Anaesthesiol. Belg. 60 (2009) 7–17.
[7] Z. Liu, Y. Wang, X. Ma, L. Zhang, C. Wang, Role of epidural fat in the local milieu: what we know and what we don't, Connect. Tissue Res. 65 (2024) 102–116.
[8] E.O. Alonge, C. Guo, Y. Wang, H. Zhang, The mysterious role of epidural fat tissue in spine surgery: a comprehensive descriptive literature review, Clin. Spine Surg. 36 (2023) 1–7.
[9] G.W. Lee, M.S. Seo, K.K. Kang, S.K. Oh, Epidural fat-derived mesenchymal stem cell: first report of epidural fat-derived mesenchymal stem cell, Asian Spine J. 13 (2019) 361–367.
[10] X. Dou, T. Mao, Y. Ma, F. Jia, Y. Liu, X. Liu, Fibrotic and inflammatory characteristics of epidural fat adjacent to the ossification area in patients with ossification of the ligament flavum, JOR Spine 5 (2022) e1229.
[11] R. Mei, W. Qin, Y. Zheng, Z. Wan, L. Liu, Role of adipose tissue derived exosomes in metabolic disease, Front. Endocrinol. 13 (2022) 873865.
[12] B. Yue, H. Wang, X. Cai, J. Wang, Z. Chai, W. Peng, S. Shu, C. Fu, J. Zhong, Adipose-secreted exosomes and their pathophysiologic effects on skeletal muscle, Int. J. Mol. Sci. 23 (2022) 12411.
[13] K. Arhiptsov, G. Marom, Numerical models of spinal cord trauma: the effect of cerebrospinal fluid pressure and epidural fat on the results, J. Neurotrauma 38 (2021) 2176–2185.
[14] J.H. Huang, C.H. Fu, Y. Xu, X.M. Yin, Y. Cao, F.Y. Lin, Extracellular vesicles derived from epidural fat-mesenchymal stem cells attenuate NLRP3 inflammasome activation and improve functional recovery after spinal cord injury, Neurochem. Res. 45 (2020) 760–771.
[15] S.E. Sung, M.S. Seo, Y.I. Kim, K.K. Kang, J.H. Choi, S. Lee, M. Sung, S.G. Yim, J.H. Lim, H.G. Seok, S.Y. Yang, G.W. Lee, Human epidural AD-MSC exosomes improve function recovery after spinal cord injury in rats, Biomedicines 10 (2022) 678.
[16] S. Shah, S. Mudigonda, T.M. Underhill, P.T. Salo, A.P. Mitha, R.J. Krawetz, Prx1 + and Hic1+ mesenchymal progenitors are present within the epidural fat and dura mater and participate in dural injury repair, Stem Cell. Transl. Med. 11 (2022) 200–212.
[17] D. Cushnie, J.C. Urquhart, K.R. Gurr, F. Siddiqi, C.S. Bailey, Obesity and spinal epidural lipomatosis in cauda equina syndrome, Spine J. : official journal of the North American Spine Society 18 (2018) 407–413.

[18] C. Crewe, Y.A. An, P.E. Scherer, The ominous triad of adipose tissue dysfunction: inflammation, fibrosis, and impaired angiogenesis, J. Clin. Invest. 127 (2017) 74–82.
[19] R. Sabaratnam, D.R. Hansen, P. Svenningsen, White adipose tissue mitochondrial bioenergetics in metabolic diseases, Rev. Endocr. Metab. Disord. (2023) 1121–1133.
[20] P.D. Talukdar, U. Chatterji, Transcriptional co-activators: emerging roles in signaling pathways and potential therapeutic targets for diseases, Signal Transduct. Targeted Ther. 8 (2023) 427.
[21] H. Yamahata, K. Osuka, T. Aoyama, M. Yasuda, H. Tokimura, K. Arita, M. Takayasu, Expression of the JAK/STAT signaling pathway in the ligamentum flavum of patients with lumbar spinal canal stenosis, J. Orthop. Sci. : official journal of the Japanese Orthopaedic Association 22 (2017) 190–196.
[22] A.Y. Huang, L. Shu, Z. Chen, C. Zhang, IL-6 is involved in thoracic ossification of the ligamentum flavum, PLoS One 17 (2022) e0272357.
[23] D. Fan, Z. Chen, Y. Chen, Y. Shang, Mechanistic roles of leptin in osteogenic stimulation in thoracic ligament flavum cells, J. Biol. Chem. 282 (2007) 29958–29966.
[24] W. Ju, A. Hoffmann, K. Verschueren, P. Tylzanowski, C. Kaps, G. Gross, D. Huylebroeck, The bone morphogenetic protein 2 signaling mediator Smad1 participates predominantly in osteogenic and not in chondrogenic differentiation in mesenchymal progenitors C3H10T1/2, J. Bone Miner. Res. : the official journal of the American Society for Bone and Mineral Research 15 (2000) 1889–1899.
[25] M. Urata, S. Kokabu, T. Matsubara, G. Sugiyama, C. Nakatomi, H. Takeuchi, S. Hirata-Tsuchiya, K. Aoki, Y. Tamura, Y. Moriyama, Y. Ayukawa, M. Matsuda, M. Zhang, K. Koyano, C. Kitamura, E. Jimi, A peptide that blocks the interaction of NF-κB p65 subunit with Smad4 enhances BMP2-induced osteogenesis, J. Cell. Physiol. 233 (2018) 7356–7366.
[26] R. Pirchio, C. Graziadio, A. Colao, R. Pivonello, R.S. Auriemma, Metabolic effects of prolactin, Front. Endocrinol. 13 (2022) 1015520.
[27] J. Li, K. Murao, H. Imachi, X. Yu, T. Muraoka, J.B. Kim, T. Ishida, Prolactin regulatory element-binding protein involved in cAMP-mediated suppression of adiponectin gene, J. Cell Mol. Med. 14 (2010) 1294–1302.
[28] W.C. Lee, A.R. Guntur, F. Long, C.J. Rosen, Energy metabolism of the osteoblast: implications for osteoporosis, Endocr. Rev. 38 (2017) 255–266.
[29] C. Zhang, Z. Chen, X. Meng, M. Li, L. Zhang, A. Huang, The involvement and possible mechanism of pro-inflammatory tumor necrosis factor alpha (TNF-α) in thoracic ossification of the ligamentum flavum, PLoS One 12 (2017) e0178986.
[30] M.M. Bhargava, E. Kinne-Saffran, R.K. Kinne, R.F. Warren, J.A. Hannafin, Characterization of sulfate, proline, and glucose transport systems in anterior cruciate and medial collateral ligament cells, Can. J. Physiol. Pharmacol. 83 (2005) 1025–1030.
[31] J. Li, L. Yu, S. Guo, Y. Zhao, Identification of the molecular mechanism and diagnostic biomarkers in the thoracic ossification of the ligamentum flavum using metabolomics and transcriptomics, BMC Mol. Cell Bio. 21 (2020) 37.
[32] F. Nian, Y. Qian, F. Xu, M. Yang, H. Wang, Z. Zhang, LDHA promotes osteoblast differentiation through histone lactylation, Biochem. Biophys. Res. Commun. 615 (2022) 31–35.
[33] V.K. Mootha, C.M. Lindgren, K.F. Eriksson, A. Subramanian, S. Sihag, J. Lehar, P. Puigserver, E. Carlsson, M. Ridderstråle, E. Laurila, N. Houstis, M.J. Daly, N. Patterson, J.P. Mesirov, T.R. Golub, P. Tamayo, B. Spiegelman, E.S. Lander, J.N. Hirschhorn, D. Altshuler, L.C. Groop, PGC-1alpha-responsive genes involved in oxidative phosphorylation are coordinately downregulated in human diabetes, Nat. Genet. 34 (2003) 267–273.
[34] A. Subramanian, P. Tamayo, V.K. Mootha, S. Mukherjee, B.L. Ebert, M.A. Gillette, A. Paulovich, S.L. Pomeroy, T.R. Golub, E.S. Lander, J.P. Mesirov, Gene set enrichment analysis: a knowledge-based approach for interpreting genome-wide expression profiles, Proc. Natl. Acad. Sci. U.S.A. 102 (2005) 15545–15550.